Extreme Mechanics Letters 45 (2021) 101276

Contents lists available at ScienceDirect

Extreme Mechanics Letters

journal homepage: www.elsevier.com/locate/eml

Moving Morphable Components-based inverse design formulation for quantum valley/spin hall insulators

Jiachen Luo, Zongliang Du *, Chang Liu *, Yue Mei, Weisheng Zhang, Xu Guo

State Key Laboratory of Structural Analysis for Industrial Equipment, Department of Engineering Mechanics, Dalian University of Technology, Dalian 116023, China
International Research Center for Computational Mechanics, Dalian University of Technology, Dalian 116023, China
Ningbo Institute of Dalian University of Technology, Ningbo 315016, China

ARTICLE INFO

Article history:
Received 13 December 2020
Received in revised form 1 February 2021
Accepted 7 March 2021
Available online 17 March 2021

Keywords:
Wave manipulation
Topological insulators
Topology optimization
Unified formulation

ABSTRACT

Supplying topologically protected wave propagation immune to backscattering, design of novel materials analogous to topological insulators is of great interest in different physical systems. Most of the related studies relies on designer's intuition or pre-knowledge, and is achieved through a trail-and-error process. In order to present a unified and rational design approach applicable to quantum valley/spin Hall insulators (QVHIs/QSHIs), a mathematical programming is proposed by combining the band theory and the Moving Morphable Components (MMC) topology optimization method. The key idea is to directly obtain a pair of unit cells with both reverse-ordered gapped Dirac cones and maximized working bandwidth through the optimization process. This design paradigm can be generalized for the systematic design of optimized 2D/3D topological insulators among different physical systems.

1. Introduction

Topological insulators (TIs), as a new type of quantum matter, distinguish from ordinary insulators in terms of possessing topologically protected edge or surface states robust against disorder and defects [1,2]. The topology origin of such extraordinary ability is some quantized values or topological invariants, e.g., Chern number or Zak phase, and this principle can be extended to other physical systems such as photonics and phononics [3,4]. Besides remarkable experiments based on topological properties, e.g., directional acoustic antennas [5], highly efficient photonic laser system [6], the properties and potential applications of topological insulators in phononic and photonic systems are highly interested [7–14].

Among topological insulators, quantum valley Hall insulators (QVHIs) and quantum spin Hall insulators (QSHIs), do not require an extra magnetic field and attract much more attention [1,2]. Due to the bulk-edge correspondence, a waveguide composed by QVHIs/QSHIs with different topological invariants, would produce an topologically protected edge state near the interface [15–17]. In most literature, the design of QVHIs/QSHIs relies on designer's intuition and is carried out by manually tuning the geometric parameters of candidates. Specifically, a symmetric unit cell with one-/two- fold Dirac cone needs to be first presented as a critical state for QVHIs/QSHIs. Then by breaking the symmetry in different manners, the Dirac cone are lifted bidirectionally and a pair of topological insulator candidates can be obtained. Finally, the topological properties of the candidates are verified by waveguide test or calculating the topological invariants. Although clear, the manually tuning process of geometry of candidates relies on designer's intuition and cognition, and this classical design method desires improvement on the rationality of tuning process and the optimality of design result.

Recently, structural topology optimization, which aims at finding the optimal distribution of materials in some prescribed domain by solving mathematical programming [18], has been successfully applied for the systematic design of novel structures and materials, including topological insulators [19–24]. Nanthakumar et al. [19] adopted level set method to design unit cells with two-fold Dirac cone to enhance the classical design procedure for QSHIs. Christiansen et al. [20,21] obtained a pair of trivial and non-trivial QSHIs by optimizing the wave propagation path in a novel photonic waveguide. The local density of state (LDOS) and a special excitation source are adopted to obtain photonic and acoustic QSHIs with extra-wide bandgaps [22,24]. To address the physical requirement and practical performance, Du et al. [23] used explicit topology optimization method to design optimized mechanical QVHIs through achieving band inversion

* Corresponding authors at: State Key Laboratory of Structural Analysis for Industrial Equipment, Department of Engineering Mechanics, Dalian University of Technology, Dalian 116023, China.
E-mail addresses: zldu@dlut.edu.cn (Z. Du), c.liu@dlut.edu.cn (C. Liu).

https://doi.org/10.1016/j.eml.2021.101276
2352-4316/

and maximizing the working bandwidth of the supercell simultaneously. Although attractive results were obtained, however, there still lacks a unified formulation applicable for different kinds of topological insulators.

In order to develop an efficient systematic inverse design method applicable for different quantum Hall effects, we adopt the Moving Morphable Component (MMC) method [25–27] to describe the multi-phase photonic crystals with specific symmetries. By extracting the quantitative requirements from the fact "a pair of desired QVHIs/QSHIs has the band structures with gapped Dirac cones in reverse order", a unified formulation is proposed to maximize the working bandwidth of the topological edge mode. Optimized QVHIs/QSHIs can be directly obtained by solving the corresponding mathematical programming. The topologically protected wave propagation of the optimized designs is verified by full wave simulation as well.

The rest of this letter is organized as follows. In Section 2, a unified formulation for inverse design of QVHIs and QSHIs are proposed combining the band theory and explicit topology optimization method. Then such design paradigm is applied for optimal photonic QVHIs and QSHIs in Section 3 and Section 4, verified by the topological wave propagation. Finally, some concluding remarks are provided at Section 5.

2. A unified mathematical formulation for inverse design of the QVHI/QSHI

It is desired to directly obtain a pair of QVHIs/QSHIs by solving a mathematical formulation. The design variables describe the unit cells, computationally tractable constraints are extracted from the physical requirements about topological property, and the design objective is to maximize the working bandwidth of the topological edge band in the corresponding waveguide.

2.1. Unit cells described by MMCs

Due to the explicit geometrical description, unit cells with specific symmetry can be described efficiently using MMCs with fewer design variables. Without loss of generality, as illustrated by Fig. 1, for a C_3-symmetric hexagon photonic crystal, the scatter medium inside the primitive cell (i.e., the dashed parallelogram) is described by the Boolean operation of totally $s = 2$ MMCs, and each MMC is determined by $l = 6$ control lines $OP_1, \ldots, OP_l$. The boundary of jth MMC in ith unit cell is determined a set of geometrical parameters including: $x_0^{[ij]}, y_0^{[ij]} \in [0, 1]$ denoting the normalized central coordinates, $\rho_m^{[ij]}$ denoting the length of the mth control line OP_m, the anti-clockwise angle $\phi^{[ij]}$ measured from line Ox to the line OP_1, and $N^{[i]}$ linear interpolating lines distributed between adjacent control lines. Besides, as shown in Fig. 1(c), the truncation $T^{[i]}$ for an adjustment of interface of the corresponding supercell is also introduced to enlarge the working bandwidth of topological edge band [28].

By this means, a pair of topological insulator candidates is described by the design variable vector $\boldsymbol{D} = \left(x_0^{[ij]}, y_0^{[ij]}, \rho_1^{[ij]}, \ldots, \rho_l^{[ij]}, \phi^{[ij]}, T^{[i]}, N^{[i]}\right)^\top, i = 1, 2, j = 1, \ldots, s$. We adopt Genetic Algorithm (GA) to obtain the design variables in present work, by taking the advantage of a fewer number of design variables in explicit topology optimization method [23,25–27].

2.2. A unified formulation for optimal QVHIs/QSHIs

According to the bulk-edge correspondence, the topological edge state can be predicted by topological invariants [1,2], while the computational complexity of the topological invariants restricts its application in the optimization formulation. An alternative way is to trace the evolution of Dirac cone in band structure, or in other words, a pair of desired QVHIs/QSHIs has the band structures with gapped Dirac cone in reverse order [1–4,15,29,30]. Here we decompose this criterion into two separate requirements expressed by the corresponding constraints respectively, i.e.,

(1) For each TI, specifically, it is obtained by breaking appropriate symmetry and the Dirac cone becomes gapped. This requirement can be denoted as a constraint $R_{\text{self}}(\boldsymbol{D}) \le 0$, where $R_{\text{self}}(\boldsymbol{D})$ is a constraint of each unit cell itself, to guarantee there exists a gapped Dirac cone in the band structure of TI candidates.

(2) In addition, the TI pair should have reversed-order band structures or achieve band inversion. We can also introduce a constraint denoted as $R_{\text{joint}}(\boldsymbol{D}) \le 0$, where $R_{\text{joint}}(\boldsymbol{D})$ is a constraint related to the unit cell together, to guarantee the topological properties of the pair of TI candidates are different.

Following Du et al.'s suggestion [23], the working bandwidth of the topological edge band of the corresponding supercell, i.e., $W(\boldsymbol{D})$, is maximized in the optimal TIs' model.

Then we can present the unified formulation of the optimal QVHIs/QSHIs as:

$$\begin{aligned} \min_{\boldsymbol{D}\subset\mathscr{U}_{\boldsymbol{D}}} \quad & -W(\boldsymbol{D}) \\ \text{s.t.} \quad & \Delta\Phi(\boldsymbol{D}) + k_0^2\Phi(\boldsymbol{D}) = \boldsymbol{0} \\ & R_{\text{self}}(\boldsymbol{D}) \le 0 \\ & R_{\text{joint}}(\boldsymbol{D}) \le 0 \end{aligned} \tag{1}$$

where $\mathscr{U}_{\boldsymbol{D}}$ is the admissible set of design variable vector; Φ denotes the wave function, which can be the pressure field $\boldsymbol{p}$ in acoustics, or the displacement field $\boldsymbol{u}_z$ for out-of-plane elastic wave, or the electric field $\boldsymbol{E}_z$ for transverse magnetic (TM) wave or $\boldsymbol{H}_z$ for transverse electric (TE) wave, respectively; and k_0 denotes the wave number. The exact expressions of $\boldsymbol{R}_{\text{self}}$ and $\boldsymbol{R}_{\text{joint}}$ will be presented later. The flowchart for solving this unified formulation is presented in Appendix.

3. Optimal design of QVHIs

For the QVHIs, as shown in Fig. 2(a) and (c), the appearance of gapped Dirac cone is induced by breaking the lattice's parity reversal symmetry, e.g., the absence of inversion or mirror symmetry [30]. Therefore, for the hexagonal lattice here, the proper symmetries can be C_3 and C_{3v}.

3.1. Formulation

The constraint $R_{\text{self}}(\boldsymbol{D}) \le 0$ is to require the pair of unit cell both has a gapped Dirac cone in their band structures. Obviously, for the eigenmodes corresponding to the vertices of the gapped Dirac cone, the phase gradient has a clear vortex [15,29], as shown in Fig. 2(b) and (d). For the nth bandgap, this feature is adopted as the requirement of appearance of a gapped Dirac cone through defining:

$$R_{\text{self}} \triangleq \bar{R}_1^{\text{V}} - R_1^{\text{V}} = \bar{R}_1^{\text{V}} - \min(\tau_{1,n}, \tau_{2,n}, \tau_{1,n+1}, \tau_{2,n+1}) \tag{2}$$

with $\tau_{i,n}$ denoting the phase gradient of the nth eigenmode of ith unit cell at K point calculated by

$$\tau_{i,n} = \frac{1}{|\Omega|}\left|\iint_{\Omega} \frac{\nabla\theta_{i,n}\cdot\boldsymbol{e}_t}{|\nabla\theta_{i,n}|} dS\right| \tag{3}$$

where $\theta_{i,m}$ is the phase distribution of the eigenmode of the ith unit cell at K point in the mth band; $\boldsymbol{e}_t = \frac{(-y,x)}{\sqrt{x^2+y^2}}$ is the unit tangent vector with respect to the line connecting the point (x, y)

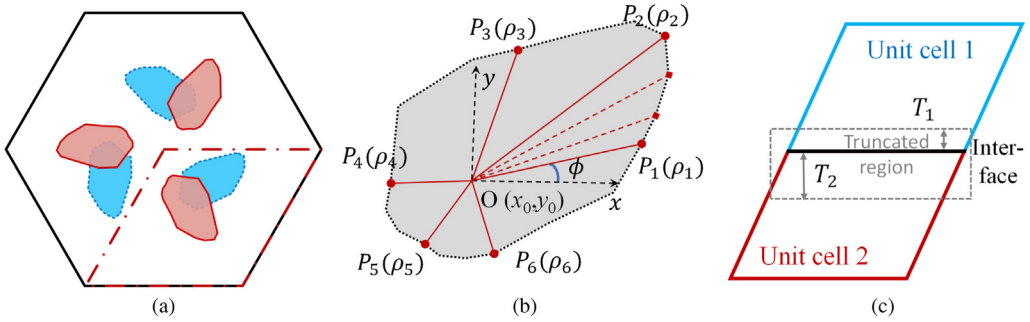

Fig. 1. Illustration of a TI candidate described by the MMC method. (a) A C_3-symmetric hexagon lattice and its primitive cell containing $s = 2$ MMCs; (b) a MMC in the primitive cell with $l = 6$ control lines (red-solid lines) and $N = 2$ linear interpolation lines (red-dashed lines) distributed between adjacent control lines. Here, point O is the original point of a component with coordinates (x_0, y_0); ρ_i is the length of ith control line OP_i; ϕ is the anti-clockwise rotation angle from x axis to OP_1; (c) the two unit cells are truncated by a distance of T_1 and T_2 near the interface of supercell respectively. (For interpretation of the references to color in this figure legend, the reader is referred to the web version of this article.)

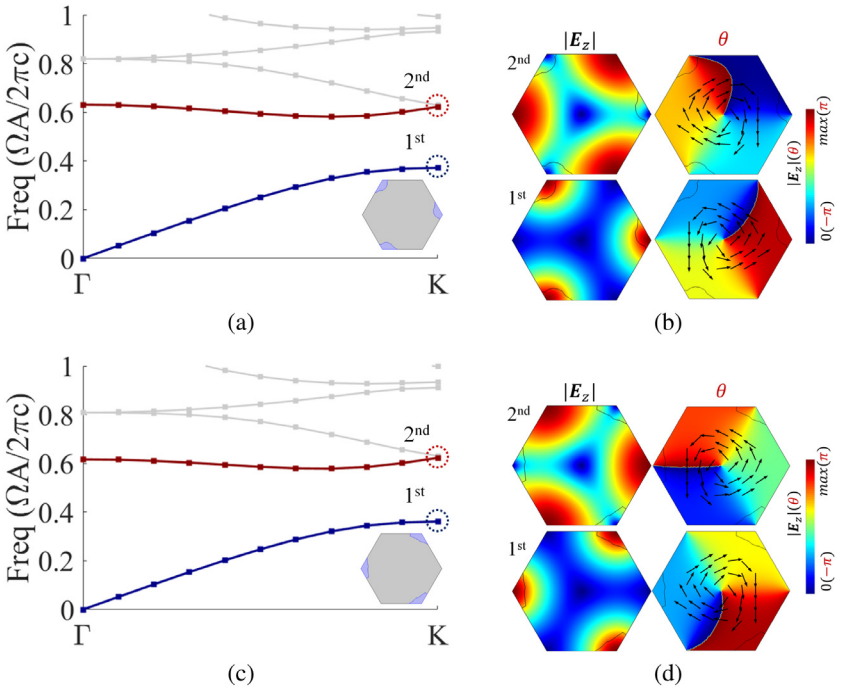

Fig. 2. Optimized QVHIs. (a) and (c) Band structures of the pair of QVHIs; (b) and (d) the field $|\boldsymbol{E}_z|$ and the phase distribution θ of QVHIs at K points of the gapped Dirac cone. Arrows illustrate the phase gradient $\nabla\theta$. The frequency is normalized by the lattice constant A and the light velocity in vacuum c. (For interpretation of the references to color in this figure legend, the reader is referred to the web version of this article.)

and the center of the lattice. The symbol $\bar{R}_1^{\mathrm{V}}$ denotes a normalized upper bound and is elaborated in Appendix.

The constraint $R_{\mathrm{joint}}(\boldsymbol{D}) \leq 0$ is to guarantee the two QVHIs have reversed-ordered band structures. This condition can also be described by the band inversion phenomenon [29], as shown in Fig. 2(b) and (d). Therefore, we can propose a normalized function for this requirement:

$$\begin{aligned} R_{\mathrm{joint}}(\boldsymbol{D}) &\triangleq \bar{R}_2^{\mathrm{V}} - R_2^{\mathrm{V}} \\ &= \bar{R}_2^{\mathrm{V}} - \min(\left\langle |\boldsymbol{\Phi}_{1,n}|, |\boldsymbol{\Phi}_{2,n+1}| \right\rangle, \left\langle |\boldsymbol{\Phi}_{1,n+1}|, |\boldsymbol{\Phi}_{2,n}| \right\rangle) \end{aligned} \tag{4}$$

where $|\boldsymbol{\Phi}_{i,m}|$ is the normalized amplitude field of eigenmode of ith unit cell at K point in mth band; $\langle\cdot,\cdot\rangle$ denotes the inner product symbol; and $\bar{R}_2^{\mathrm{V}}$ is a normalized upper bound detailed in Appendix.

By substituting Eqs. (2) and (4) into Eq. (1), one can obtain the exact mathematical programming for optimal design of QVHIs.

3.2. Optimal designs

For the TM wave, the unit cells are assumed to be C_3-symmetric and composed by air ($\epsilon_r^{\mathrm{air}} = 1, \mu_r^{\mathrm{air}} = 1$) and ($\epsilon_r^{\mathrm{Si}} = 11.7$, $\mu_r^{\mathrm{Si}} = 1$) for Silicon [29]. By setting $\bar{R}_1^{\mathrm{V}} = 0.85$ and $\bar{R}_2^{\mathrm{V}} = 0.4$, Eq. (1) is solved to obtain optimal QVHIs discretized by adaptive mesh using commercial software COMSOL 5.2a and Matlab 2013a starting from a random initial guess. Parameters of GA algorithms are available in Appendix.

Fig. 2(a) and (c) illustrate the two optimized QVHIs with gapped Dirac cones in band structures. From Fig. 2(b) and (d), obviously, clear vortices exist in all those eigenmodes related to gapped Dirac cone, and band inversion is achieved between these two designs. The effectiveness of the proposed constraints is verified.

To further validate the topological interface state, a ribbon-shaped supercell shown in Fig. 3(b) is studied. As illustrated by Fig. 3(a), an upper-edge state band (colored in red solid line) has a normalized working frequency range of 0.370–0.455 (about 0.085), which is wider than the bandwidth of intuition-based design in literature [29] (about 0.028). The edge states and zoomed power flow of the inset points shown in Fig. 3(b) reveal the energy is intensively localized at the interface of the optimized QVHIs. Fig. 3(c) plots the transmission spectra of a straight waveguide and a waveguide with a sharp corner. By

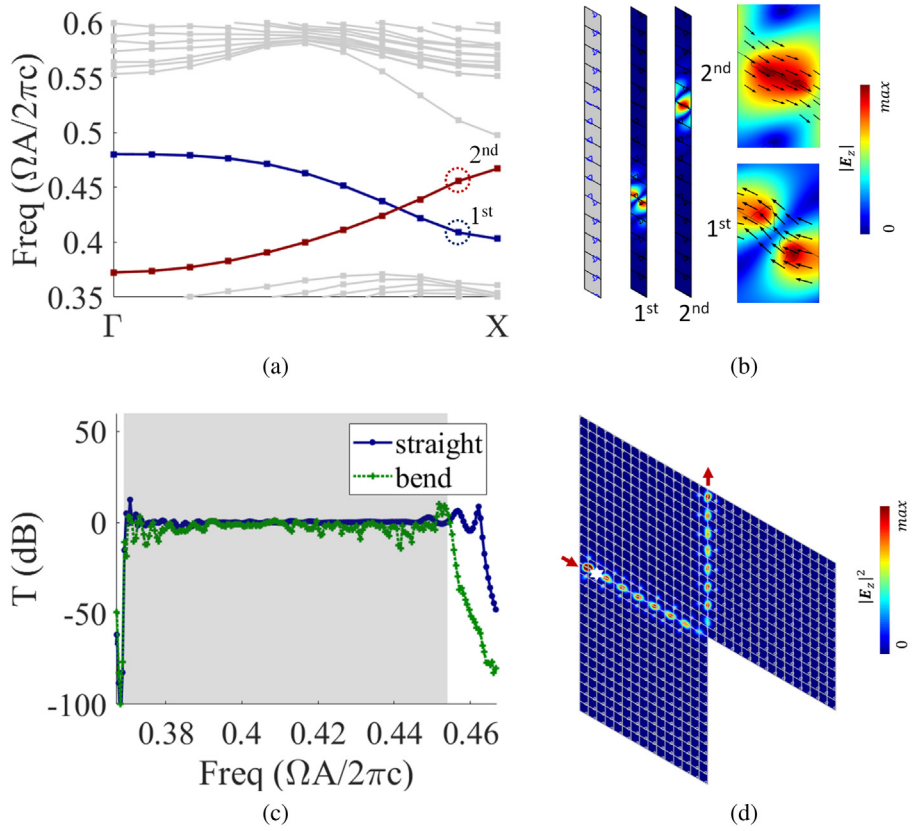

Fig. 3. (a) The band structure of the ribbon-shaped QVHI supercell (the upper/lower-edge state is colored by the red/blue line); (b) the geometry, the upper-edge state, lower-edge state and the zoomed power flow; (c) the transmission spectra and (d) $|\boldsymbol{E}_z|^2$ in the corresponding waveguides by full wave simulation. (For interpretation of the references to color in this figure legend, the reader is referred to the web version of this article.)

exciting a line source of frequency 0.400 at the left side of waveguide illustrated by Fig. 3(d), the light can robustly reach the top side with almost no-backscattering.

4. Optimal design of QSHIs

As revealed by former studies [16,17], the quantum spin Hall effect can be created by lifting a double Dirac cone, which is an accidental degeneracy of the 2-fold $p_\pm$ and 2-fold $d_\pm$ bands (see Fig. 4(a)–(d) for reference). Generally, unit cells with C_6 or C_{6v} symmetry are candidates of hexagonal QSHIs.

4.1. Formulation

To guarantee the existence of a gapped double Dirac cone, for a nth band, the 2-fold degeneracy is adopted as a constraint:

$$R_{\text{self}} \triangleq R_1^S - \bar{R}_1^S = \max(d_{1,n}, d_{2,n}, d_{1,n+2}, d_{2,n+2}) - \bar{R}_1^S \le 0 \tag{5}$$

where $d_{i,n}$ denote the distance between the $(n-1)$th and nth band of ith unit cell at Γ point.

For the constraint $R_{\text{joint}}(\boldsymbol{D}) \le 0$ about the order-reversal property of band structures of a pair of QSHIs, the band inversion requirement is still effective. Specifically, it is expressed as

$$R_{\text{joint}}(\boldsymbol{D}) \triangleq \bar{R}_2^S - R_2^S = \bar{R}_2^S - \min(I_1, I_2) \tag{6}$$

with

$$\begin{aligned} I_1 = \min\{ & \max\left(\left\langle|\Phi_{1,n-1}|, |\Phi_{2,n+1}|\right\rangle, \left\langle|\Phi_{1,n-1}|, |\Phi_{2,n+2}|\right\rangle\right), \\ & \max\left(\left\langle|\Phi_{1,n}|, |\Phi_{2,n+1}|\right\rangle, \left\langle|\Phi_{1,n}|, |\Phi_{2,n+2}|\right\rangle\right)\} \\ I_2 = \min\{ & \max\left(\left\langle|\Phi_{1,n+1}|, |\Phi_{2,n-1}|\right\rangle, \left\langle|\Phi_{1,n+1}|, |\Phi_{2,n}|\right\rangle\right), \\ & \max\left(\left\langle|\Phi_{1,n+2}|, |\Phi_{2,n-1}|\right\rangle, \left\langle|\Phi_{1,n+2}|, |\Phi_{2,n}|\right\rangle\right)\} \end{aligned}$$

By substituting Eqs. (5) and (6) into Eq. (1), one can obtain the exact formulation for optimal design of QSHIs. The bounds $\bar{R}_1^S$, $\bar{R}_2^S$ for QSHIs are determined in Appendix.

4.2. Optimal designs

For TM wave, the unit cells are assumed to be C_6-symmetric and composed by air and Silicon as well. For simplicity in geometry, there is only one MMC in the primitive cell (i.e., an equilateral triangle). Except for $\bar{R}_1^S = 10^{-3}$ and $\bar{R}_2^S = 0.75$, the same parameters as those for the optimal design of QVHIs are used unless otherwise stated.

Fig. 4(a) and (c) present the optimized QSHIs and their band structures with a 2-fold degeneracy at the Γ point. For the trivial and non-trivial QSHIs, the band inversion about $p_\pm$ and $d_\pm$ states are illustrated by Fig. 4(b) and (d), respectively. These features imply the order-reversal gapped double Dirac cones as well as the topological properties in the QSHIs are successfully guaranteed by solving the proposed mathematical programming.

Furthermore, the band structure of the ribbon-shaped supercell shown in Fig. 5(b) is investigated. A topological spin-up band of upper edge (i.e., colored in red solid line in Fig. 5(a)) is observed with a normalized working bandwidth from 0.485 to 0.548 (about 0.063), which is slightly wider than the optimized result in literature [22] (about 0.058) as well. The corresponding edge states and zoomed power flow of the inset point are shown in Fig. 5(b). Obviously, the energy is flowing up and strongly localized at the interface in Fig. 5(b). As illustrated in Fig. 5(d), applying a spin-down excitation with normalized frequency of 0.504 at the middle of QSHIs' interface, light only propagates down to the right port as expected and the transmission spectra is Fig. 5(c).

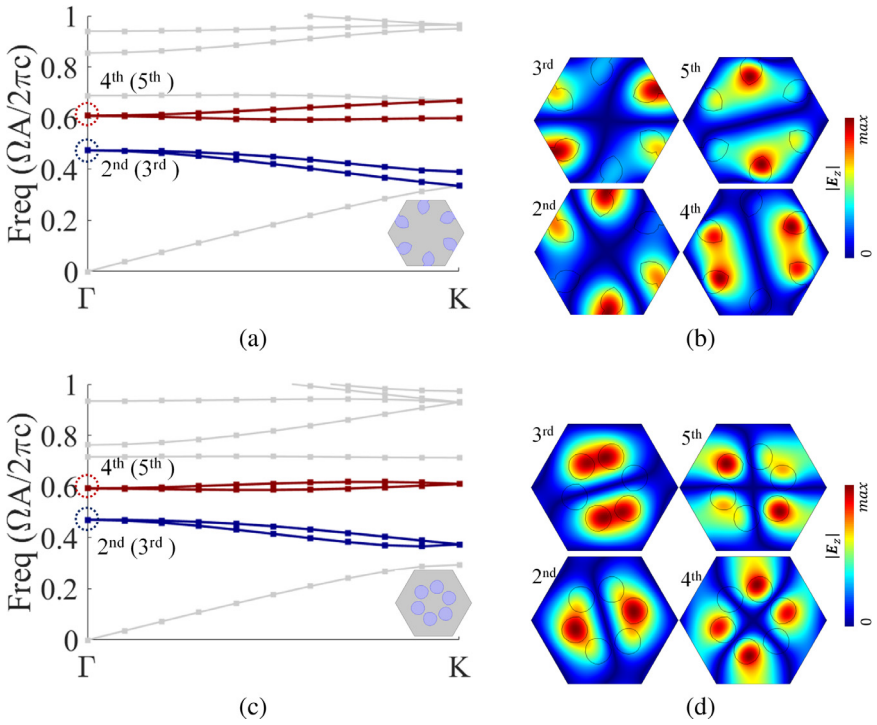

Fig. 4. Optimized QSHIs. (a) and (c) Band structures of the pair of QSHIs; (b) and (d) the field $|\boldsymbol{E}_z|$ of QSHIs at Γ points of the gapped Dirac cone. (For interpretation of the references to color in this figure legend, the reader is referred to the web version of this article.)

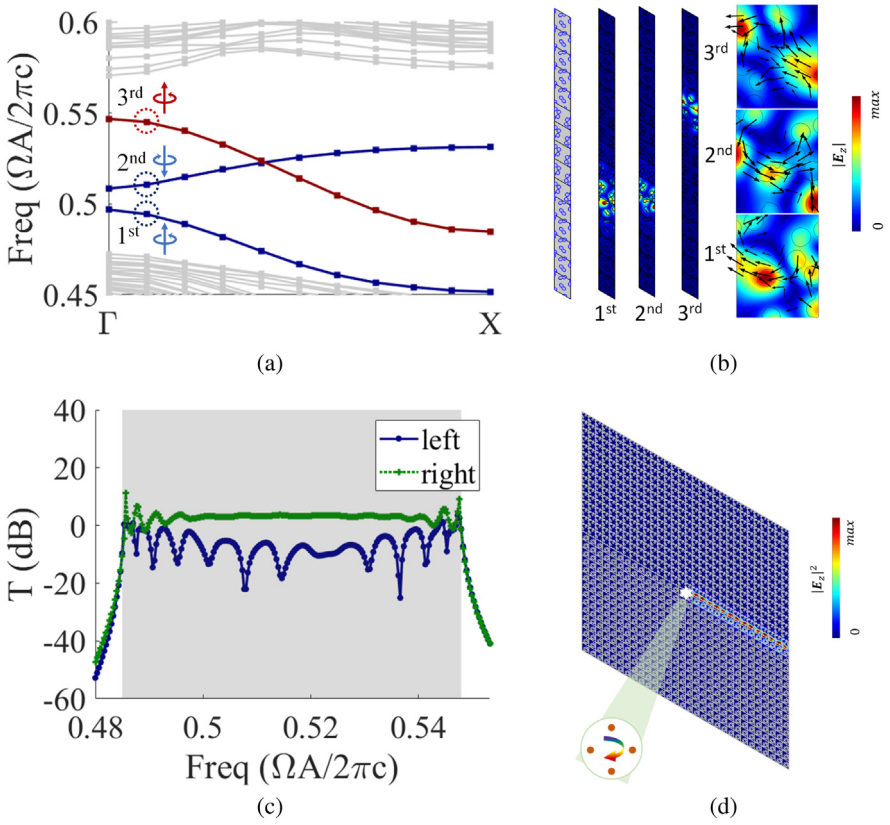

Fig. 5. (a) The band structure of the ribbon-shaped QSHI supercell (the upper/lower-edge state is colored by the red/blue line); (b) the geometry, the upper-edge state, lower-edge state and the zoomed power flow; (c) the transmission spectra and (d) $|\boldsymbol{E}_z|^2$ in the corresponding waveguides by full wave simulation. (For interpretation of the references to color in this figure legend, the reader is referred to the web version of this article.)

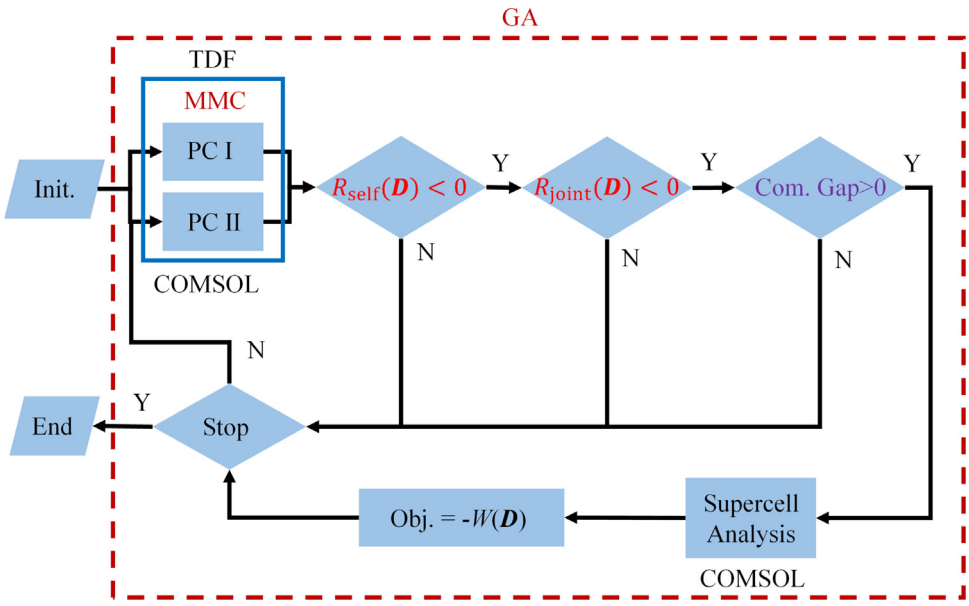

Fig. 6. Flowchart of solving the unified formulation for optimal design of QVHIs and QSHIs.

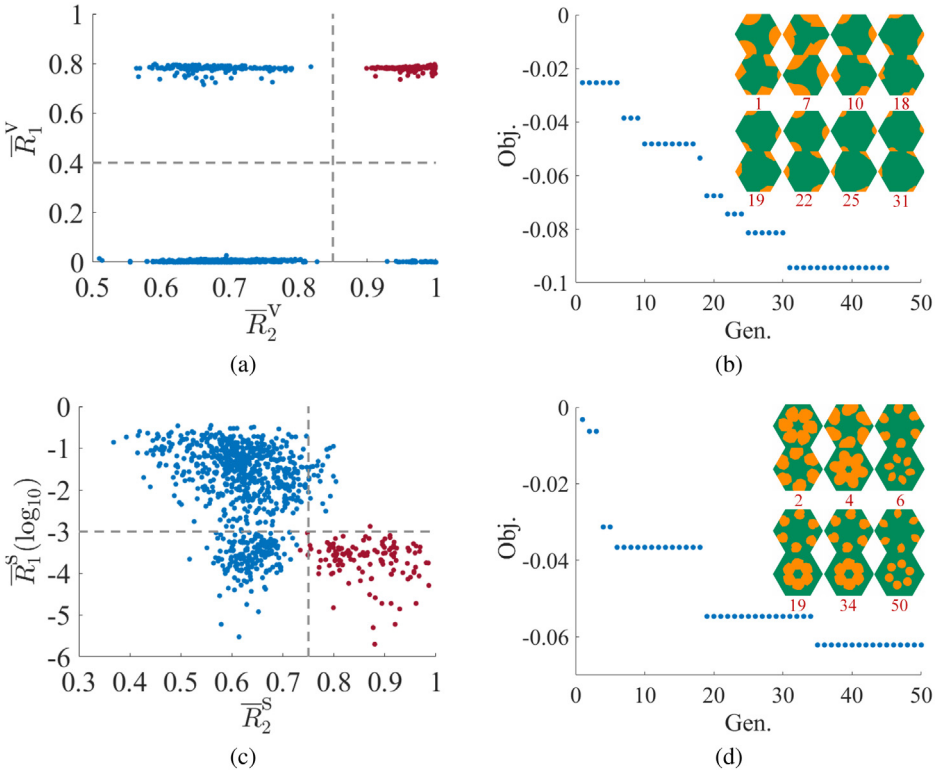

Fig. 7. (a) and (c) Determining the bounds $(\bar{R}_1^V, \bar{R}_2^V)$ and $(\bar{R}_1^S, \bar{R}_2^S)$ by random sampling, where the red points correspond to TI pairs with desired topological properties; (b) and (d) iteration history and some intermediate designs of optimal QVHIs and QSHIs with Silicon colored in yellow. (For interpretation of the references to color in this figure legend, the reader is referred to the web version of this article.)

5. Conclusion

In this letter, based on the band theory, a unified topology optimization formulation is proposed for the inverse design of insulators with different topological effects. It is validated that, a pair of QVHIs/QSHIs with maximized working bandwidth can be directly obtained by solving the corresponding mathematical programming, without depending on the designer's intuition nor the trail-and-error tuning process. The corresponding topologically protected wave propagation is verified by full wave simulation. With the help of 3D-MMC based topology optimization method [31,32], this design paradigm is also applicable for the inverse design of 3D topological insulators and TIs in other physical systems. Future work will be focused on extending this design framework for rational design of other topological materials, e.g., higher-order topological insulators and semi-metals.

Declaration of competing interest

The authors declare that they have no known competing financial interests or personal relationships that could have appeared to influence the work reported in this paper.

Availability of data

The data that support the findings of this study are available from the corresponding authors upon reasonable request.

Acknowledgments

This work is supported by the National Natural Science Foundation of China (11821202, 11732004, 12002073, 12002077, 12002075, 11922204, 11872141), the National Key Research and Development Plan, China (2020YFB1709401, 2016YFB0201601), the Fundamental Research Funds for the Central Universities, China (Grant No. DUT20RC(3)020, DUT19RC(3)017), Liaoning Revitalization Talents Program, China (XLYC1907119), Postdoctoral Science Foundation, China funded project (2020T130078, 2020M680944), Program for Changjiang Scholars, Innovative Research Team in University (PCSIRT), China and 111 Project, China (B14013).

Appendix

The flowchart for solving the proposed unified formulation is illustrated in Fig. 6.

To determine the bounds $\bar{R}_1^{\mathrm{V}}, \bar{R}_2^{\mathrm{V}}$ and $\bar{R}_1^{\mathrm{S}}, \bar{R}_2^{\mathrm{S}}$, 1000 pairs of random designs are obtained by sampling the design variable vector. The corresponding values of $R_1^{\mathrm{V}}, R_2^{\mathrm{V}}$ and $R_1^{\mathrm{S}}, R_2^{\mathrm{S}}$ are scattered in Fig. 7(a) and (c), respectively. The points colored in red correspond to TI designs with order-reversal gapped Dirac cone and are well-separated with other points with respect to $\bar{R}_1^{\mathrm{V}} = 0.4$, $\bar{R}_2^{\mathrm{V}} = 0.85$ and $\bar{R}_1^{\mathrm{S}} = 10^{-3}$, $\bar{R}_2^{\mathrm{S}} = 0.75$.

The parameters for GA setting are: the population size 100, the crossover fraction 0.8, the migration fraction 0.2, the elite count 5, the stall generation limit 15 and the fitness function tolerance 10^{-4}. The iteration history and some intermediate designs of optimized QVHIs and QSHIs are presented in Fig. 7(b) and (d).

References

[1] M.Z. Hasan, C.L. Kane, Colloquium: Topological insulators, Rev. Modern Phys. 82 (4) (2010) 3045–3067.
[2] X. Qi, S.-C. Zhang, Topological insulators and superconductors, Rev. Modern Phys. 83 (4) (2011) 1057–1110.
[3] T. Ozawa, H.M. Price, A. Amo, N. Goldman, M. Hafezi, L. Lu, M.C. Rechtsman, D. Schuster, J. Simon, O. Zilberberg, et al., Topological photonics, Rev. Modern Phys. 91 (1) (2019) 015006.
[4] G. Ma, M. Xiao, C.T. Chan, Topological phases in acoustic and mechanical systems, Nat. Rev. Phys. 1 (4) (2019) 281–294.
[5] Z. Zhang, Y. Tian, Y. Wang, S. Gao, Y. Cheng, X. Liu, J. Christensen, Directional acoustic antennas based on Valley-Hall topological insulators, Adv. Mater. 30 (36) (2018) 1803229.
[6] M.A. Bandres, S. Wittek, G. Harari, M. Parto, J. Ren, M. Segev, D.N. Christodoulides, M. Khajavikhan, Topological insulator laser: Experiments, Science 359 (6381) (2018).
[7] H. Chen, H. Nassar, G. Huang, A study of topological effects in 1D and 2D mechanical lattices, J. Mech. Phys. Solids 117 (2018) 22–36.
[8] Q. Zhang, Y. Chen, K. Zhang, G. Hu, Programmable elastic valley Hall insulator with tunable interface propagation routes, Extreme Mech. Lett. 28 (2019) 76–80.
[9] Q. Wu, H. Chen, X. Li, G. Huang, In-plane second-order topologically protected states in elastic kagome lattices, Phys. Rev. A 14 (1) (2020) 014084.
[10] H. Al Ba'ba'a, K. Yu, Q. Wang, Elastically-supported lattices for tunable mechanical topological insulators, Extreme Mech. Lett. (2020) 100758.
[11] W. Zhou, B. Wu, Z. Chen, W. Chen, C. Lim, J. Reddy, Actively controllable topological phase transition in homogeneous piezoelectric rod system, J. Mech. Phys. Solids 137 (2020) 103824.
[12] Y. Yang, Z. Gao, H. Xue, L. Zhang, M. He, Z. Yang, R. Singh, Y. Chong, B. Zhang, H. Chen, Realization of a three-dimensional photonic topological insulator, Nature 565 (7741) (2019) 622–626.
[13] E. Lustig, S. Weimann, Y. Plotnik, Y. Lumer, M.A. Bandres, A. Szameit, M. Segev, Photonic topological insulator in synthetic dimensions, Nature 567 (7748) (2019) 356–360.
[14] L. Zhang, Y. Yang, Z.-K. Lin, P. Qin, Q. Chen, F. Gao, E. Li, J.-H. Jiang, B. Zhang, H. Chen, Higher-order topological states in surface-wave photonic crystals, Adv. Sci. 7 (6) (2020) 1902724.
[15] T. Ma, G. Shvets, All-Si valley-Hall photonic topological insulator, New J. Phys. 18 (2) (2016) 025012.
[16] L. Wu, X. Hu, Scheme for achieving a topological photonic crystal by using dielectric material, Phys. Rev. Lett. 114 (22) (2015) 223901.
[17] Z. Zhang, Q. Wei, Y. Cheng, T. Zhang, D. Wu, X. Liu, Topological creation of acoustic pseudospin multipoles in a flow-free symmetry-broken metamaterial lattice, Phys. Rev. Lett. 118 (8) (2017) 084303.
[18] M.P. Bendsoe, O. Sigmund, Topology Optimization: Theory, Methods, and Applications, Springer Science & Business Media, 2013.
[19] S. Nanthakumar, X. Zhuang, H.S. Park, C. Nguyen, Y. Chen, T. Rabczuk, Inverse design of quantum spin Hall-based phononic topological insulators, J. Mech. Phys. Solids 125 (2019) 550–571.
[20] R.E. Christiansen, F. Wang, O. Sigmund, Topological insulators by topology optimization, Phys. Rev. Lett. 122 (23) (2019) 234502.
[21] R.E. Christiansen, F. Wang, O. Sigmund, S. Stobbe, Designing photonic topological insulators with quantum-spin-Hall edge states using topology optimization, Nanophotonics 8 (8) (2019) 1363–1369.
[22] Y. Chen, F. Meng, B. Jia, G. Li, X. Huang, Inverse design of photonic topological insulators with extra-wide bandgaps, Phys. Status Solidi (RRL)–Rapid Res. Lett. 13 (9) (2019) 1900175.
[23] Z. Du, H. Chen, G. Huang, Optimal quantum valley Hall insulators by rationally engineering berry curvature and band structure, J. Mech. Phys. Solids 135 (2020) 103784.
[24] H.-W. Dong, S.-D. Zhao, R. Zhu, Y.-S. Wang, L. Cheng, C. Zhang, Customizing acoustic dirac cones and topological insulators in square lattices by topology optimization, J. Sound Vib. 493 (2020) 115687.
[25] X. Guo, W. Zhang, W. Zhong, Doing topology optimization explicitly and geometrically—a new moving morphable components based framework, J. Appl. Mech. 81 (8) (2014) 081009.
[26] W. Zhang, W. Yang, J. Zhou, D. Li, X. Guo, Structural topology optimization through explicit boundary evolution, J. Appl. Mech. 84 (1) (2017) 011011.
[27] R. Xue, R. Li, Z. Du, W. Zhang, Y. Zhu, Z. Sun, X. Guo, Kirigami pattern design of mechanically driven formation of complex 3D structures through topology optimization, Extreme Mech. Lett. 15 (2017) 139–144.
[28] Y. Deng, H. Ge, Y. Tian, M. Lu, Y. Jing, Observation of zone folding induced acoustic topological insulators and the role of spin-mixing defects, Phys. Rev. B 96 (18) (2017) 184305.
[29] X.-D. Chen, F.-L. Zhao, M. Chen, J.-W. Dong, Valley-contrasting physics in all-dielectric photonic crystals: Orbital angular momentum and topological propagation, Phys. Rev. B 96 (2) (2017) 020202.
[30] N. Lera, D. Torrent, P. San-Jose, J. Christensen, J.V. Alvarez, Valley Hall phases in kagome lattices, Phys. Rev. B 99 (13) (2019) 134102.
[31] W. Zhang, D. Li, J. Yuan, J. Song, X. Guo, A new three-dimensional topology optimization method based on moving morphable components (MMCs), Comput. Mech. 59 (4) (2017) 647–665.
[32] W. Zhang, J. Chen, X. Zhu, J. Zhou, D. Xue, X. Lei, X. Guo, Explicit three dimensional topology optimization via moving morphable void (MMV) approach, Comput. Methods Appl. Mech. Engrg. 322 (2017) 590–614.